Sliding spool design for reducing the actuation forces in direct operated proportional directional valves: Experimental validation

Sliding spool design for reducing the actuation forces in direct operated proportional directional valves: experimental validation

Riccardo Amirante[*°], Elia Distaso[*], Paolo Tamburrano[*]

* Department of Mechanics, Mathematics and Management (DMMM),
Polytechnic University of Bari, Italy

° corresponding author's contact information:
amirante@poliba.it – tel. +390805963470 – fax. +390805963411

Abstract

This paper presents the experimental validation of a new methodology for the design of the spool surfaces of four way three position direct operated proportional directional valves. The proposed methodology is based on the re-design of both the compensation profile (the central conical surface of the spool) and the lateral surfaces of the spool, in order to reduce the flow forces acting on the spool and hence the actuation forces. The aim of this work is to extend the application range of these valves to higher values of pressure and flow rate, thus avoiding the employment of more expensive two stage configurations in the case of high-pressure conditions and/or flow rate. The paper first presents a theoretical approach and a general strategy for the sliding spool design to be applied to any four way three position direct operated proportional directional valve. Then, the proposed approach is experimentally validated on a commercially available valve using a hydraulic circuit capable of measuring the flow rate as well as the actuation force over the entire spool stroke. The experimental results, performed using both the electronic driver provided by the manufacturer and a manual actuation system, show that the novel spool surface requires remarkably lower actuation forces compared to the commercial configuration, while maintaining the same flow rate trend as a function of the spool position.

Keywords: flow force reduction, proportional valves, direct actuation, experimental validation

Nomenclature

A	Valve port connected to the actuator
A_r	Area of the metering section [mm^2]
B	Valve port connected to the actuator
$C_{d,A-T1}$	Discharge coefficient of the metering section A-T_1

$C_{d,P-B}$	Discharge coefficient of the metering section P-B
$C_{d,V}$	Overall discharge coefficient
D	Diameter of the compensation profile [mm]
F_{act}	Actuation force [N]
F_{el}	Elastic force [N]
F_{flow}	Flow force [N]
$F_{flow,centre}$	Flow force acting on the central chamber [N]
$F_{flow,left}$	Flow force acting on the left chamber [N]
$F_{flow,right}$	Flow force acting on the right chamber [N]
$F_{transient}$	Transient flow force [N]
h	Length of the lateral cylindrical surfaces [mm]
k	Length of the lateral conical surfaces [mm]
l	Length of the compensation profile [mm]
$\dot{m}$	Mass flow rate [kg/s]
$\dot{\mathrm{m}}_{T1}$	Mass flow rates of the fluid flow discharged through port T_1 [kg/s]
$\dot{\mathrm{m}}_{T2}$	Mass flow rates of the fluid flow discharged through port T_2 [kg/s]
P	Valve port connected to the pump
T	Valve port connected to the tank
$(V_A)_x$	Average axial velocity at the inlet of the left control volume [m/s]
$(V_B)_x$	Average axial velocity at the outlet of the central control volume [m/s]
$(V_P)_x$	Average axial velocity at the inlet of the central control volume [m/s]
V_r	Velocity in the metering section [m/s]
$(V_T)_x$	Average axial velocity at the outlet of the left control volume [m/s]
$(V_{T2})_x$	Average axial velocity at the inlet of the right control volume [m/s]

$(V_{T2}{}')_x$	Average axial velocity at the outlet of the right control volume [m/s]
x	Spool position [mm]

Greek

Δp_{B-T}	Pressure drop B-T
Δp_{P-A}	Pressure drop P-A
Δp_v	Pressure drop across the valve [N/m^2]
ρ	Fluid density [kg/m^3]

1. Introduction

Hydraulic directional proportional valves are usually employed to modulate the flow rate through an actuator (hydraulic cylinder or hydraulic motor) with high precision in an attempt to control the stationary velocity and the position of the actuator as well as its acceleration and deceleration, while maintaining high simplicity of the hydraulic circuit employed.

Proportional directional valves are of two types: direct operated valves and two stage valves. The former configuration, in which proportional solenoids are used to move the valve spool directly, allows the achievement of higher response speeds by virtue of the direct actuation and is cheaper thanks to a lower number of mechanical and electrical parts. Unfortunately, the direct actuation is not possible in the case of high values of mass flow rate and/or pressure because, in these conditions, the flow forces acting on the spool are too high to be counteracted by the electromagnetic forces generated by commercially available solenoids. As a result, in spite of the remarkable increase in costs and worsening of response times, the two stage configuration is mandatory when the mechanical power required by the hydraulic actuator is high.

A current research field aims at reducing the complexity and costs of two stage valves by proposing novel configurations for the first stage. In fact, the complexity of a two stage valve is due to the first stage serving as a hydraulic amplifier, which can be a flapper nozzle, a deflector jet or a sliding spool;

the hydraulic amplifier generates a force unbalance on the extremities of the second stage spool which is forced to move and in turn allows flow modulation in the hydraulic circuit. The electromagnetic force, responsible for the actuation of the first stage, can be provided by either an electromagnetic torque motor (in the case of deflector jets and nozzle-flappers [1]) or a solenoid (in the case of first stage sliding spools). In this regard, a recent research paper proposed a novel first stage concept that uses a piezoelectric actuator in place of the conventional electromagnetic torque motor [1]; the experimental and Computational Fluid Dynamics (CFD) analysis presented in [1] demonstrated that the concept is viable and that the use of the piezoelectric actuation can reduce the weight and complexity as well as costs of two stage valves. Moreover, an investigation into piezoelectric ring benders and their potential for actuating servo valves was presented in [2], providing an insight into how such actuators may be mounted for use as actuators in servo valve pilot stages.

Another research field aims at improving the performance of standard configurations of two stage valves by using CFD in an attempt to gain a more comprehensive understanding of the flow features within these valves. This is made possible by the high accuracy reached by current numerical strategies, which are capable of effectively predicting the stationary flow (see, e.g., the CFD setting proposed by Chattopadhyay et al. [3]) as well as the dynamic spool movement inside hydraulic valves (in this regard, the paper by Saha et al. is noteworthy [4]). This advancement is due both to the high effectiveness of the commercially available CFD software packages and to the high level of competence matured by the above-mentioned authors in handling these commercial software packages, as seen through their published literature (e.g. see [5]).

Such effective numerical strategies are also used to study new kinds of valves. As an example, CFD methods were employed to simulate the dynamic characteristics of a pilot-control globe valve [6], which is a new kind of valve with simple structures and low driving energy consumption [7].

With regard to standard configurations of two stage valves, the most studied one is that employing the flapper-nozzle amplifier. Aung et al. [8] presented a very detailed investigation into the flow forces and energy loss characteristics of five possible flapper–nozzle structures with three different null clearances. Taking advantage of their simulation results, Pan et al. [9] succeeded in retrieving a formula for the discharge coefficient of flapper-nozzle valves under laminar, transitional and turbulent conditions. A partially 3D CFD analysis was performed in [10] to study cavitation in the flapper-nozzle pilot stage, showing that the curved edge of traditionally used flapper shapes is responsible for the occurrence of cavitation. Furthermore, an innovative flapper shape was proposed in [10] that significantly reduces cavitation. The effectiveness of rectangle-shaped flappers in reducing cavitation was experimentally confirmed in [11] by comparison with more traditional flapper shapes. Also cavity shedding dynamics in flapper–nozzle pilot stages were investigated experimentally and numerically in [12]. An innovative flapper shape was proposed and validated both experimentally and numerically in [13], in order to reduce the undesired lateral forces acting on the flappers of flapper–nozzle pilot valves, which can interfere with the stability of the flappers. Another recent paper proposed replacing pilot operated directional control valves with suitable logic valves [14]; the paper showed that the design of proper body units consisting of logic valves can produce a significant reduction in pressure losses, namely up to 61%, in the analyzed hydraulic system [14].

All the abovementioned research papers have contributed to enhancing the potential of two stage valves, providing novel concepts, numerical studies and optimized shapes for the design of the hydraulic amplifier. Contrarily, the authors of this paper have concentrated all efforts on a different strategy, which is focused on direct operated proportional directional valves and aims at enlarging their operation field, rather than reducing the complexity and drawbacks of two stage proportional directional valves. To accomplish the task of extending the application range of direct operated

proportional directional valves to higher values of pressure and flow rate, a redesign of these valves must be conceived, as they present non-optimized geometries which restrict their potential, as also highlighted by Herakovic [15]. He proved that it is possible to reduce the flow force in a hydraulic proportional valve by implementing opportune geometrical modifications to the sliding spool and the valve socket [15]. Moreover, Simic and Herakovic [16] made effective changes both to the sliding spool and to the valve body of an ON/OFF small hydraulic seat valve, confirming that the non-optimized profiles of commercially available valves have a great influence on the required actuation forces. Herakovic et al. also provided some possible methods in [17] for reducing the static flow forces in hydraulic sliding-spool and small on/off seat valves: the results of their research are very promising and prove that the axial component of the flow forces and therefore the necessary actuation force can be reduced significantly just by modifying the geometry of the valve housing and spool. Lisowski et al. [18] also demonstrated that commercial valves do not present effective profiles: they focused on the redesign of the valve body of a commercial solenoid operated directional control valve, proposing additional channels inside the body of a control valve that can remarkably reduce the actuation forces; a very accurate CFD analysis was used to design the new valve body. Simic et al. [19] also proposed new approaches for the modelling and simulation of hydraulic spool valves by using simple mathematical expressions for describing the sliding spool geometry. A very recent paper by the same authors of this paper showed, by means of CFD and experimental investigations, that commercial spool profiles, in addition to causing large actuation forces, also cause undesired phenomena such as cavitation [20].

Other papers were focused on proposing novel control systems of direct operated valves: the coupling between optimized geometries and such optimized control techniques could further enhance the potential of direct operated directional valves. In this regard, with the objective of improving the dynamics of direct operated proportional directional valves, Amirante et al. [21]

proposed a novel open loop control technique, which is based on the coupling between the peak and hold technique and the pulse width modulation (PWM). Jin et al. [22] employed a differential control method based on differential signals simultaneously delivered to both solenoids of a direct operated proportional valve to enhance the frequency response of the valve.

In this scenario, this paper proposes a strategy for improving the sliding spool surfaces of typical 4/3 directional proportional direct operated valves, with the aim of reducing the actuation forces without changing the operation characteristics (i.e. maximum flow rate and flow rate vs opening degree). This paper is focused only on the improvement in the spool geometry, with the valve body being kept unchanged. In order to demonstrate the effectiveness of the proposed methodology, this paper presents the experimental comparison between a commercially available proportional spool and a novel one. The latter is characterized by more effective surfaces, which are capable of reducing the flow forces while maintaining the same flow rate characteristics (i.e. flow rate vs spool position). The optimized spool surface has been designed for a specific commercially available valve; however, as described in the following section, the concept has general validity and can be applied to any 4/3 directional direct operated proportional valve.

2. Methodology

2.1 Improvement in the sliding spool surface: theoretical approach and general strategy

Figure 1 shows the graphic symbol of a 4/3 directional direct operated proportional valve (top) along with a sketch of its typical architecture (bottom). The proportional sliding spool is moved directly by either the right solenoid or the left solenoid depending on the required hydraulic connections (P $\rightarrow$ A, B $\rightarrow$ T or P $\rightarrow$ B, A $\rightarrow$ T). In Fig. 1 the hydraulic connections of the valve ports are P$\rightarrow$ B and A $\rightarrow$ T: the oil enters the valve through the high pressure port P, then it flows through the metering section P$\rightarrow$ B (which is determined by the metering edge of the spool) and finally exits the valve through port B. Likewise, the oil discharged from the hydraulic actuator reenters the valve through

port A and crosses the metering section A→ T_1. At this point part of the oil flows towards port T_1, while the remaining part flows within the internal axial channel of the valve towards port T_2. Ports T_1 and T_2 are externally connected (not represented in Fig. 1 for simplicity) so as to form the unique discharge port T. As demonstrated both experimentally and numerically in [20], the metering section A→ T_1 is the most critical zone of the entire valve, because the restricted passage through the notches lead to a sudden increase in flow velocity, which in turn causes the pressure to fall below the vapor pressure of the fluid, leading to the formation of vapor cavities [20].

The driving solenoid develops an actuation force (F_{act}) which is proportional to the duty cycle of the Pulse width modulation (PWM) signal applied to the coil of the solenoid. The actuation force must be capable of counteracting both the elastic force exerted by the centering springs (F_{el}) and the reaction forces acting on the spool surface due to the fluid motion, usually referred to as the flow forces (F_{flow}).

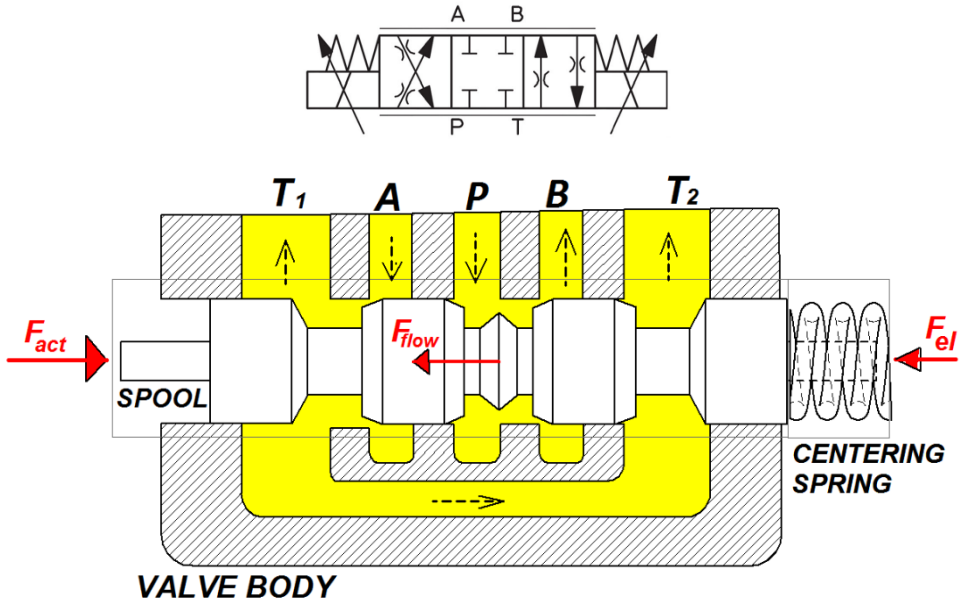

Fig.1- Symbol of a 4/3 direct operated directional proportional valve (top) and its typical geometric architecture (bottom)

The axial position assumed by the sliding spool depends on the equilibrium among the three forces (F_{act} , F_{el} , F_{flow}). Because F_{flow} significantly increases with the increasing flow rate, a high value of F_{act}

is required to obtain a high opening degree. Furthermore, for a fixed opening degree, the increase in the pressure drop P-T leads to a corresponding increase in the required actuation force (F_{act}) since the flow rate is proportional to the square root of the pressure drop [20]. As a result, the operating conditions (pressure and flow rate) must be limited to respect the maximum electromagnetic force provided by commercially available solenoids.

The described configuration is common to most commercially available 4/3 direct operated valves, and this paper proposes an effective strategy for minimizing the flow forces acting on this valve typology. Fig. 2a shows an enlargement of the section view of Fig.1, revealing that the overall flow force acting on the spool surface along the x axis is the sum of three contributions:

$$F_{flow} = F_{flow,left} + F_{flow,centre} + F_{flow,right} \quad (1)$$

The three flow force contributions are due to the interaction between the fluid and the spool within the central chamber P-B ($F_{flow,centre}$), the left chamber A-T_1 ($F_{flow,left}$) and the right chamber in correspondence of the exit T_2 ($F_{flow,right}$). The application of the conservation of momentum to the three control volumes (highlighted by three dashed rectangles in Fig.2a), with the assumption of stationary flow, allows expressing equation 1 as follows:

$$F_{flow} = \dot{m}[(V_A)_x - (V_T)_x] + \dot{m}[(V_B)_x - (V_P)_x] + \dot{m}_{T2}[(V_{T2})_x - (V_{T2}{}')_x] \quad (2)$$

Where $\dot{m}$ denotes the overall mass flow rate of the oil entering the valve, while $\dot{m}_{T1}$ and $\dot{m}_{T2}$ (where $\dot{m}_{T1} + \dot{m}_{T2} = \dot{m}$) denote the mass flow rates of the fluid flow discharged through port T_1 and port T_2, respectively; $(V_A)_x$ and $(V_T)_x$ are the average axial velocities at the inlet and outlet sections of the left control volume, respectively; $(V_B)_x$ and $(V_P)_x$ are the average axial velocities at the outlet and inlet of the central control volume, respectively; similarly, the axial components of the average velocity at the outlet and inlet of the right control volume are denoted by $(V_{T2})_x$ and $(V_{T2}{}')_x$, respectively. As the direction of the flow within the left control volume is orthogonal to the *x* axis, $(V_{T2})_x$ and $(V_{T2}{}')_x$ can be neglected, therefore equation 2 can be simplified as follows:

$$F_{flow} = \dot{m}[(V_A)_x - (V_T)_x + (V_B)_x - (V_P)_x] \quad (3)$$

192

193 The geometrical parameters that influence both $(V_A)_x$ and $(V_B)_x$ are the metering edges of the
194 spool, which can either be linear with a fixed slope (as shown in Fig. 2) or present spherical and
195 cylindrical notches as well as conical cutouts to produce a nonlinear trend of the flow rate as a
196 function of the spool position. A comprehensive analysis of the effects of the groove shapes upon
197 the flow area and velocities as well as discharge characteristics is provided in [23].
198 The values of $(V_P)_x$ and $(V_T)_x$ are determined, respectively, by the central conical surface of the
199 spool (referred to as the compensation profile) and the lateral conical surfaces of the spool.

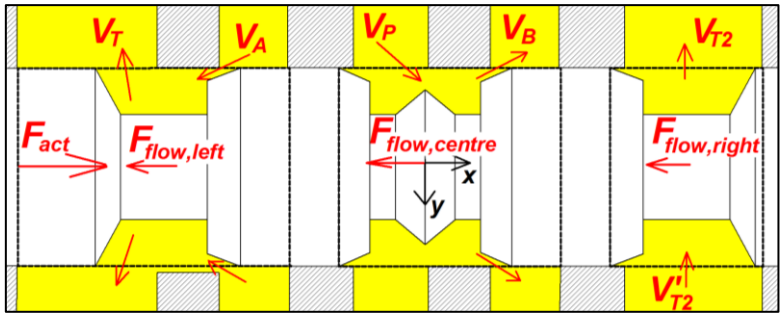

200

201 *(a)*

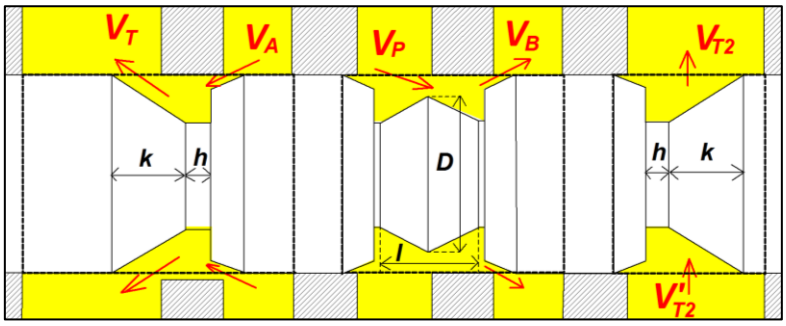

202

203 *(b)*

204 *Fig.2- velocity vectors on a non-optimized spool surface (fig.2a) and on an optimized spool surface*
205 *(fig.2b)*

206 The strategy proposed here for reducing the flow forces is focused on optimizing the compensation
207 profile (the central conical surface of the spool) and the lateral surfaces of the spool so as to increase

208 the magnitude of $(V_P)_x$ and $(V_T)_x$, while maintaining $(V_A)_x$ and $(V_B)_x$ unchanged in order not to
209 change the metering characteristics of the selected spool.
210 Fig. 2 shows a qualitative example of an optimized spool profile (Fig. 2b) compared to a non-
211 optimized one (Fig. 2a). The comparison reveals that such an optimized surface can remarkably
212 change the velocity vectors. As shown in Fig. 2b, the main geometrical features of the spool can be
213 kept unchanged (i.e. the maximum and minimum diameters, overall length and metering edges); in
214 contrast, the values of the geometrical parameters of the compensation profile, namely its diameter
215 *(D)* and length *(l)*, can properly be redesigned so as to increase the velocity magnitude and the entry
216 angle at the inlet of the central control volume, leading to a remarkably increase in $(V_P)_x$. Similarly,
217 the geometric characteristics of the lateral surfaces, namely the values of *h* and *k*, can be optimized
218 with the aim of both reducing the flow area at the exit of the metering chamber A-T_1 and decreasing
219 the exit angle formed with the x axis, thus remarkably increasing $(V_T)_x$.
220 However, it must be noted that the selection of the optimum values of *D, I, h, k* must be carried out
221 correctly to avoid an unacceptable reduction in the flow rate, for example due to either an
222 overestimation of *D* and *l* or an underestimation of the sum *h + k*. For these reasons, the selection
223 of the optimum values of *D, I, h, k* must be done at the maximum opening of the valve (or at a very
224 large opening degree), in order to avoid an undesired reduction in the flow rate. In fact, if the new
225 spool profiles do not reduce the flow rate at the large opening degrees, the flow rate at smaller
226 openings is expected to remain unchanged (compared to the commercial configuration) by virtue
227 of the unchanged metering characteristics.
228 This strategy is expected to produce the maximum beneficial effect at the large openings, because
229 the increase in both $(V_{T1})_x$ and $(V_P)_x$ will grow with the increasing opening degree. In contrast, the
230 effect of the improved spool surfaces is expected to be almost null at the small openings, because
231 the flow passages in sections P and T_1 will be too large at the small openings to produce a significant

232 increase in $(V_{T1})_x$ and $(V_P)_x$. This expected behavior is consistent with the objective of extending
233 the application range of these valves, which undergo the highest flow forces at the large openings.
234 The analysis developed so far has been concerned only with the stationary flow forces. However, it
235 is widely known that the flow force acting on the spool can be decomposed into a steady flow force
236 contribution (expressed by equation 3) and a transient one, which is generated whenever the spool
237 moves from a steady state position to another one. It can easily be demonstrated that the transient
238 flow force is not influenced by the proposed strategy. In fact, as reported in [24], the transient flow
239 force ($F_{transient}$) can be calculated for each metering chamber as follows:

$$F_{transient} = L\frac{d\dot{m}}{dt} = L\rho\frac{d(A_r V_r)}{dt} \quad (4)$$

240 Where *L* is the axial length of the metering section, *ρ* is the fluid density, V_r is the velocity in the
241 metering section and A_r is the area of the metering section. Because the proposed strategy aims at
242 maintaining the metering characteristics unchanged (both A_r and V_r), one can conclude that the
243 proposed strategy does not change $F_{transient}$ significantly; therefore, the overall actuation force
244 reduction is only due to the reduction in the stationary flow forces.

245 2.2 Application of the proposed strategy to a commercially available valve

246 The generic approach described in the previous sub-section was applied to a specific case in order
247 to evaluate its effectiveness. The selected proportional valve is the 4/3 ATOS DKZOR-T model [25],
248 whose operating principles and architecture are very similar to other commercially available
249 proportional direct operated valves. As shown in Fig. 3, the valve body (1) is made up of 5 chambers;
250 the spool (2) is direct operated by two solenoids (3) and its position is accurately measured by a
251 Linear Variable Displacement Transducer (LVDT) with a linearity error equal to ±0.15% of the full
252 scale. The electronic driver (5) supplies the driving solenoid with precise values of current that are
253 proportional to the reference signal.

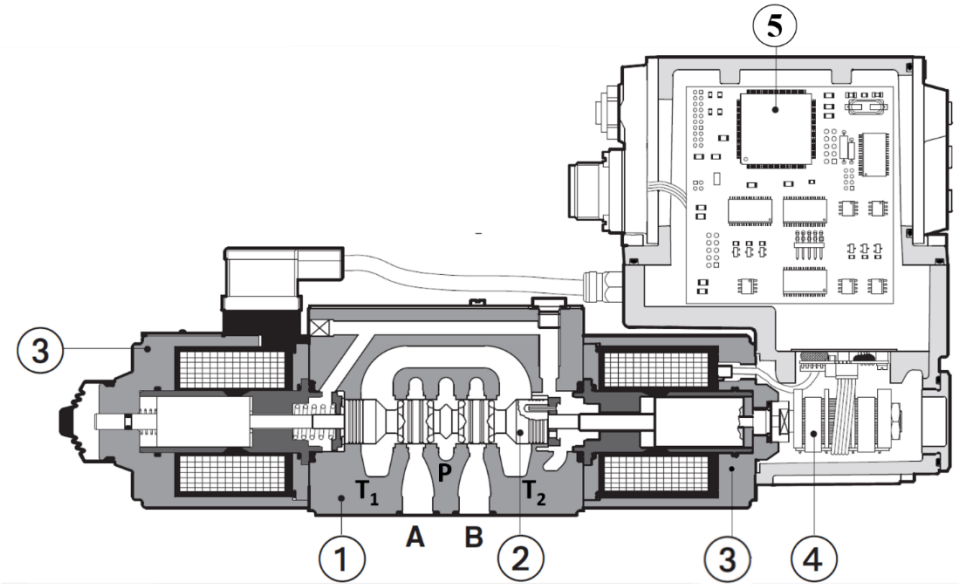

Fig.3- sketch of the valve ATOS DKZOR-T [25]
(1 = valve body , 2= spool, 3= solenoids, 4=LVDT, 5= electronic driver)

This valve can be equipped with 7 different sliding spools: four of them are linear, whereas the other three are progressive. The seven spools present different metering characteristics from one another, but have the same design as far as the compensation profile and the lateral conical surfaces are concerned.

Fig. 4 provides both a photograph and a CAD representation of the selected sliding spool, which is a progressive spool (indicated by the manufacturer as the *S3* model) capable of providing 120 l/min at the maximum opening when the pressure drop P-T is equal to 70 bar (data provided by the manufacturer). Fig. 4 shows that the progressive metering effect is achieved by means of 3 cylindrical notches and 3 spherical grooves as well as a conical cutout machined on each metering edge of the spool. This shape of the spool confers a progressive non-linear flow rate trend as a function of the spool position. In particular, the cylindrical notches coupled with the spherical grooves create the metering section at the small openings, determining a parabolic flow rate trend as a function of the spool position up to 40% of the maximum opening degree. At the larger opening degrees (from 40% of the maximum opening degree to the maximum opening), the conical cutout is uncovered by the edges of the valve body and the flow area increases linearly with the increasing

spool position; as a result, if the pressure drop P-T is maintained constant, the flow rate will increase linearly with the spool position from 40% to 100% of the maximum opening degree.

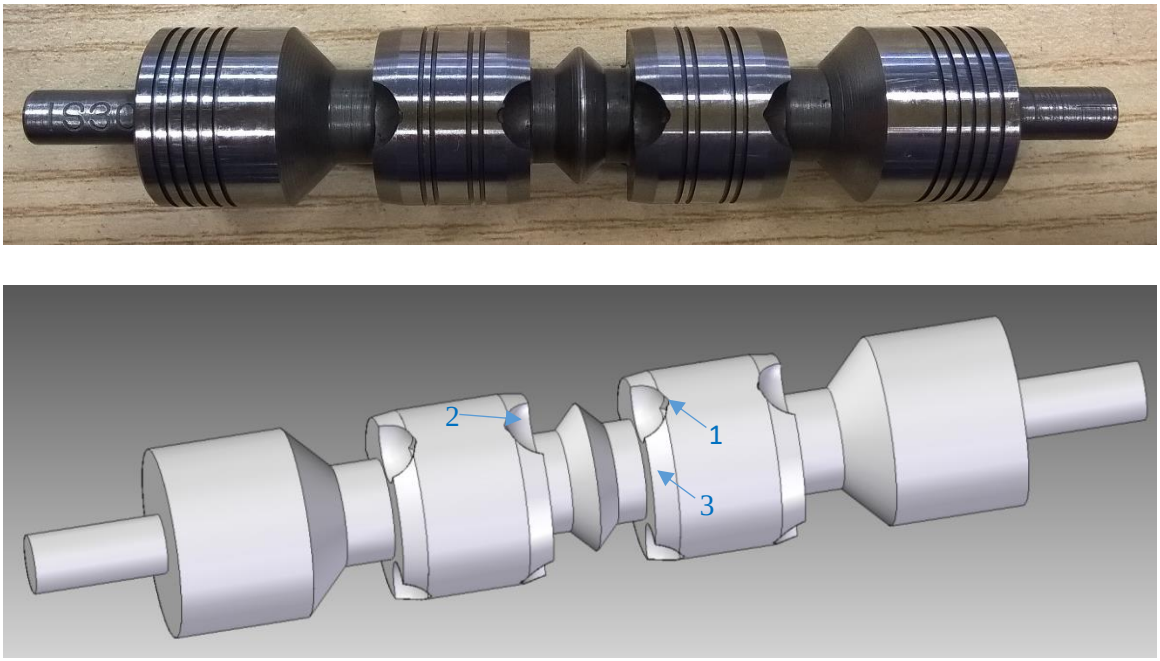

Fig.4- photograph of the commercial sliding spool and its CAD representation (1=cylindrical notch, 2= spherical groove, 3= conical cutout)

Fig 5 shows a photograph of the commercial sliding spool (Fig 5a) compared to a photograph of the improved sliding spool (fig 5b) which was conceived using the strategy described in the previous section. As mentioned earlier, all the spool parameters were maintained unchanged except for the parameters *l*, *D*, *h*, *k*, in order to maintain the same flow rate characteristics. The different values for *l*, *D*, *h*, *k* are shown qualitatively in fig. 6, which shows the CAD representations of the commercial sliding spool (6a) and of the optimized one (6b), and their specific values are reported in Table 1. The comparison between the optimized values and the commercial ones reveals that the new compensation profile has a greater axial length and a similar radius, resulting in a flow at the inlet section of the central chamber P-B more aligned with the horizontal direction compared to the

290 commercial geometry; furthermore, the new spool is characterized by different lateral conical
291 surfaces which have a more inclined edge, thus allowing the axial flow velocity at the outlet section
292 to be increased due to a smaller flow area and a greater alignment with the x axis. The new spool
293 was constructed out of the same material as the commercial one; therefore, considering that the
294 new spool has maintained the same main geometric characteristic as the commercial one (except
295 for the compensation profile and the spool extremities), the mass of the two spools are almost
296 identical, which results in the same inertia force for both spools.
297 The optimum values selected for *l, D, h, k* resulted from an optimization process based on the
298 coupling between an optimization algorithm and the fully 3D CFD modeling of the fluid flow within
299 the valve. The CFD model was described in [24], whereas the setting and results of the optimization
300 process were described in detail in [26].
301 As described in [26], the optimization process (which was implemented into the optimization
302 software modeFRONTIER) was based on the coupling between a genetic algorithm (MOGAII) and
303 the fully 3D CFD mono-phase model of the fluid flow within the valve. The efficiency of MOGA II,
304 which was also successfully used in other papers (see, e.g., Amirante et al. [27]), is due to the new
305 "directional cross-over" operator, which outperforms the classical cross-over algorithm [26].
306 The objective of the optimization process was the minimization of the flow forces at a very large
307 opening degree (2.55 mm, which is very close to the maximum opening), with the constraint being
308 the constant flow rate occurring at this opening degree. The optimization process consisted in a
309 sequential and iterative process. First, the initial population was generated by the employed DOE
310 algorithm (Sobol) with a number of individuals equal to 50. Starting with this initial population, the
311 following procedures and calculations were automatically performed to find the best geometrical
312 configuration:
313 (a) 3D representation of the individuals that respected the prescribed bounds;

(b) generation of the computational grid that discretized each new geometry (at the selected opening) by means of the grid generator software;

(c) CFD simulation, with final calculation of the flow forces;

(d) evaluation of the objective function and generation of the next population.

The process was stopped after the best geometrical configuration had remained unchanged for several generations. The best solution belonged to the 20th generation and was characterized by the parameters reported in Table1. Overall, 30 generations, and thus approximately 1500 individuals, were explored.

The CFD simulations in the optimization process were performed by setting the overall pressure drop across the valve equal to 100 bar and neglecting the pressure drop through the actuator. Although these valves are subjected to cavitation in the discharge section as demonstrated in [20], the CFD mono-phase model was employed into the optimization process. This choice is due to the fact that the employment of the mixture model (capable of predicting cavitation) in such an optimization process results to be an unreliable approach, since the mixture model requires more iterations and a remarkably longer computational time than that required by the single phase model [20].

This fluid-dynamic optimization process is a valuable tool to choose effective values for *h,k,D,L*; however, It should be noted that other approaches could be used to find effective values for *h,k,D,L* (e.g. trial and error and rapid prototyping techniques). As the final step, this paper provides the experimental comparison between the optimized sliding spool and the commercial one. Section 2.3 describes the experimental test rig assembled to perform the comparison between the two sliding spools.

5a

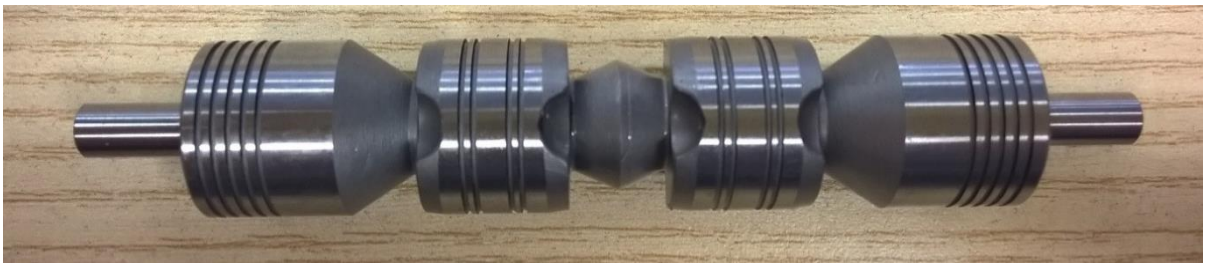

5b

Fig.5- photographs of the commercial sliding spool (fig 4a) and optimized one (fig. 4b)

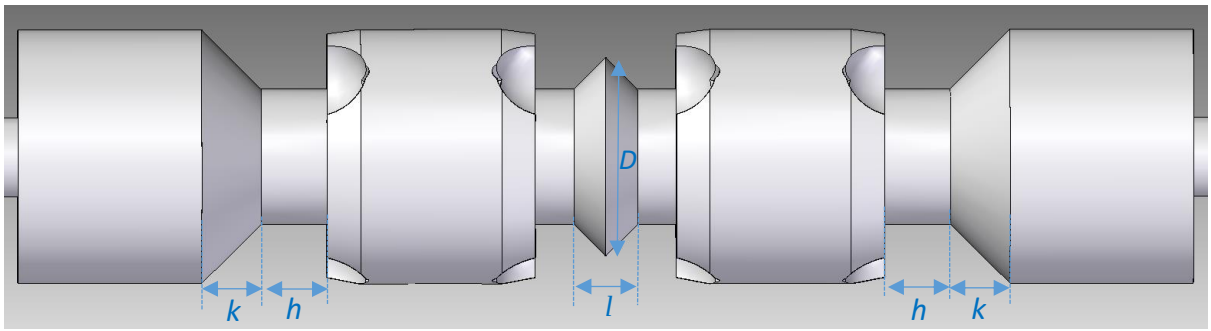

6a

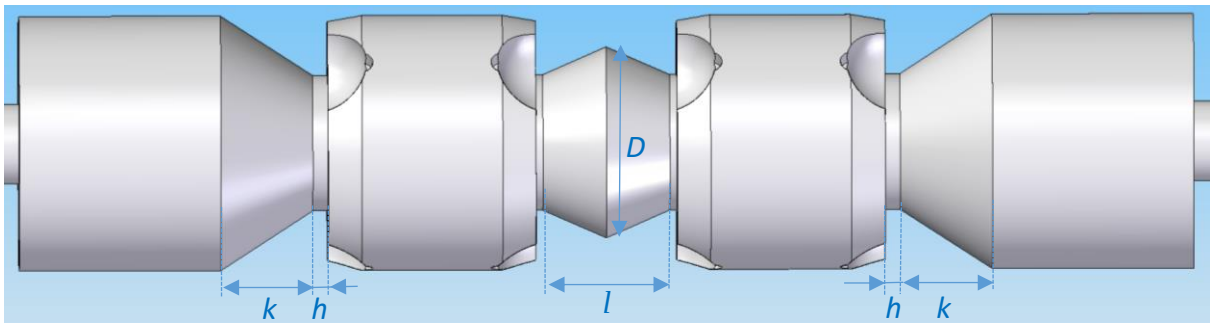

6b

Fig.6- CAD representations of the commercial sliding spool (fig 6a) and of the optimized one (fig. 6b)

	Commercial spool	Optimized spool	Difference (%)
L (mm)	4.8	8.0	+66.7
D (mm)	12.5	12.0	-4.0
h (mm)	4	0.95	-76.3
K (mm)	4	5.8	+45.0

Table 1- Reference and optimal values of the design parameters.

2.3 Experimental test rig and test typologies

In order to compare the new spool with the commercial spool of the ATOS DKZOR-T directional proportional valve, the valve was inserted in a hydraulic circuit, which allows both the flow rate and the actuation force to be accurately measured over the entire spool stroke. The measurement of the axial spool position was obtained by means of the centesimal Linear Variable Displacement Transducer the proportional directional valve is equipped with.

A photograph and the scheme of the hydraulic circuit are provided in Fig. 7. Port A and port B of the proportional directional valve (1) were connected to the VSE VS4-GPO gear flow meter (2) characterized by a measuring error lower than ±0.1% of the full scale (*150 l/min*). The proportional directional valve (1) was supplied with high pressure hydraulic oil provided by the Sauer Danfoss SNP 3/38d gear pump (3) having a maximum rotation speed of 3000 rpm and capable of generating a maximum pressure of 350 bar. The pump was driven by the A4C 200 LB2 asynchronous motor manufactured by Marelli motors (4); therefore a frequency converter controlled by the external PC was used to adjust the rotational speed of the pump. Two pressure relief valves (5,6) were placed downstream of the proportional directional valve. The ATOS AGAM-10/210/V 32 pressure relief valve (5), which is operated by means of a screw, was installed in the high pressure line with the aim of limiting the pressure in the circuit in case of the failure of the proportional pressure relief valve

(6). The latter (model: ATOS AGMZO-A-10/210/Y6/13*)* was mounted upstream of the directional valve in order to control the pressure drop P-T finely and automatically. To that end, the command signal to this valve was properly adjusted by a PID algorithm.

Four DS EUROPE LP 660 pressure transducers (7,8,9,10), with a measuring error lower than ±1% of the full scale (100 bar), were installed to measure the pressure at the four ports (P,A,B,T) of the directional valve (1). An Epoll AS/1,5/360/2,95/6,3 accumulator (11) was connected to the high pressure line in order to reduce the pressure fluctuations at port P.

A LabVIEW™ code was employed along with a 16 bit data acquisition card in order to allow control and data acquisition by means of an external computer.

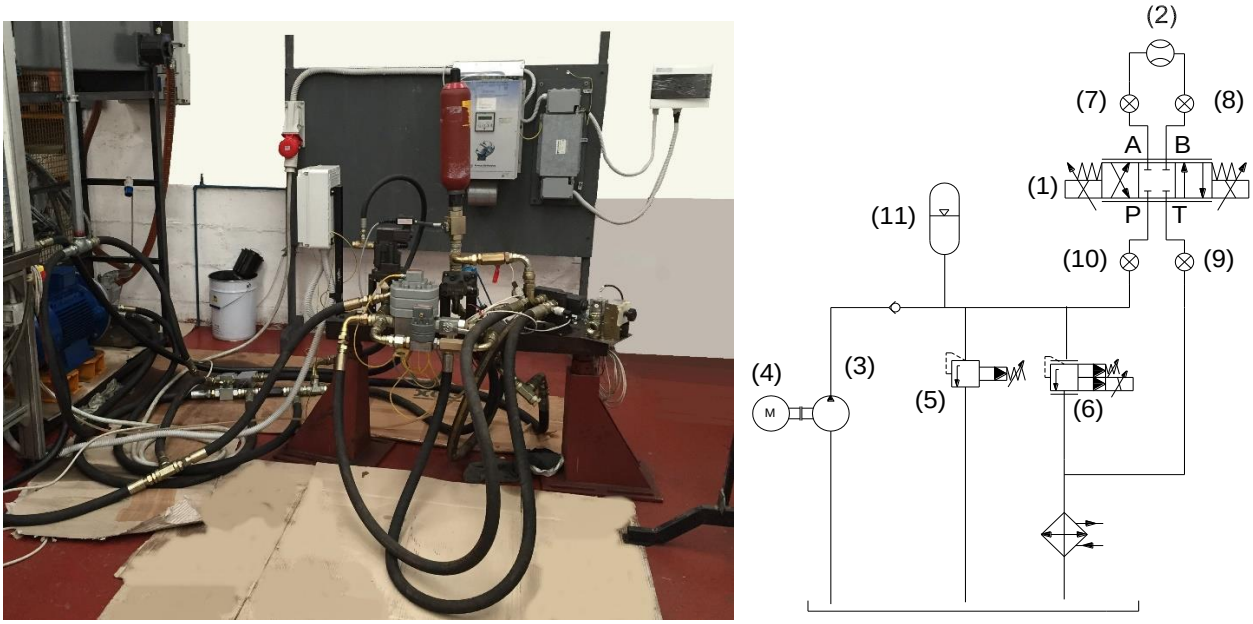

Fig.7- Photograph of the hydraulic circuit (left) and its scheme (right). Symbols: 1 Proportional directional valve (ATOS DKZOR-T); 2 Gear flow meter (VSE VS4-GPO); 3 Gear pump (Sauer Danfoss SNP 3/38d); 4 Electric motor (Marelli A4C 200 LB2); 5 Pressure relief valve (ATOS AGAM-10/210/V 32); 6 Analog controlled proportional pressure relief valve (ATOS AGMZO-A-10/210/Y6/13); 7,8,9,10 Pressure transducers at port A, B, T, P (DS EUROPE LP 660); 11 Accumulator (Epoll AS/1,5/360/2,95/6,3)

Two typologies of experimental tests were carried out on the above hydraulic test rig to quantify the driving force reduction achieved with the new spool profile in comparison with the commercial one:

1. The first test typology was conducted by using the electronic driver provided by the manufacturer, which was connected with the external PC. The driving force required to move the sliding spool inside the valve body depends both on the position of the armature inside the coil and on the current flowing through the same coil, which is usually adjusted by the electronic driver modulating the duty cycle of the constant amplitude voltage applied to the coil. This test typology consisted in supplying the electronic driver with a step voltage (control signal) set with the external PC; according to this input analog signal, the electronic driver proportionately changed the duty cycle of the pulse width modulation signal provided to the proportional valve. As a result, the change in the control signal caused a corresponding change in the current flowing through the driving solenoid, thus varying the driving force acting on the spool. These experimental tests allowed evaluating which of the two spools reached higher positions for fixed values of the control signal (voltage provided by the external PC) and fixed values of pressure drop P-T.
2. The second test typology was carried out by using a manual actuation system in place of the integrated control system provided by the manufacturer. The valve assembly underwent some modification, as shown in Fig. 8. The armature inside the coil, which is in contact with the sliding spool, was moved through a knob: a load cell, interposed between the manual actuation and the armature, allowed the actuation force to be measured. The load cell measured the axial force in the range 0÷250 N by means of an appropriate extensimeter, with the measuring error being lower than ±0.023 % of the full scale. These experimental tests allowed retrieving the actuation force (measured by the load cell) vs the spool position (measured by the LVDT) for both spools.

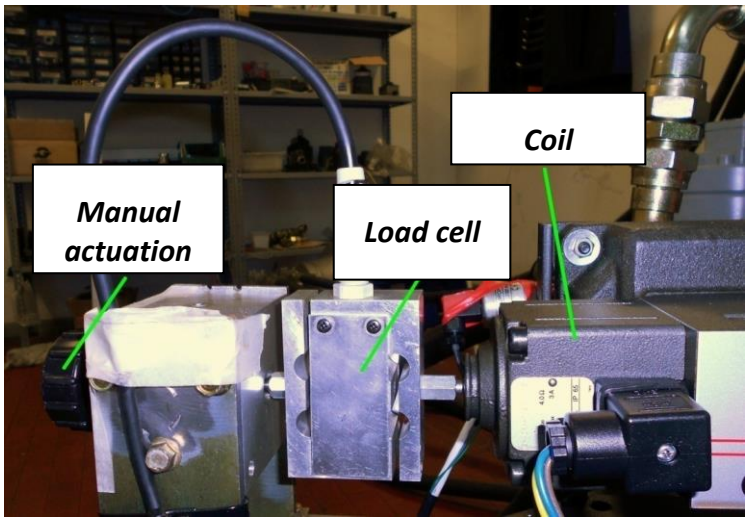

***Figure 8**- Manual actuation and measurement of the driving force*

3. Experimental results

In this section, the experimental validation of the new spool profiles is presented. To accomplish this task, the improved sliding spool (see fig.5b) was experimentally compared with the commercial one (see fig.5a); as mentioned earlier, the comparison was performed using two different test typologies.

The first test typology took advantage of the electronic driver of the valve and consisted in imposing sudden and large variations in the control signal (voltage from the computer to the driver of the valve). The sampling frequency of the data acquisition card was set equal to 50000 samples per second. These tests allowed measuring the final position reached by both spools for fixed values of the control signal and pressure drop P-T: the greater the spool position, the lower the flow forces acting on the spool and hence the lower the actuation force required to move the spool.

In order to have a reliable comparison, during the step tests the oil temperature was maintained constant and equal to about 40 °C.

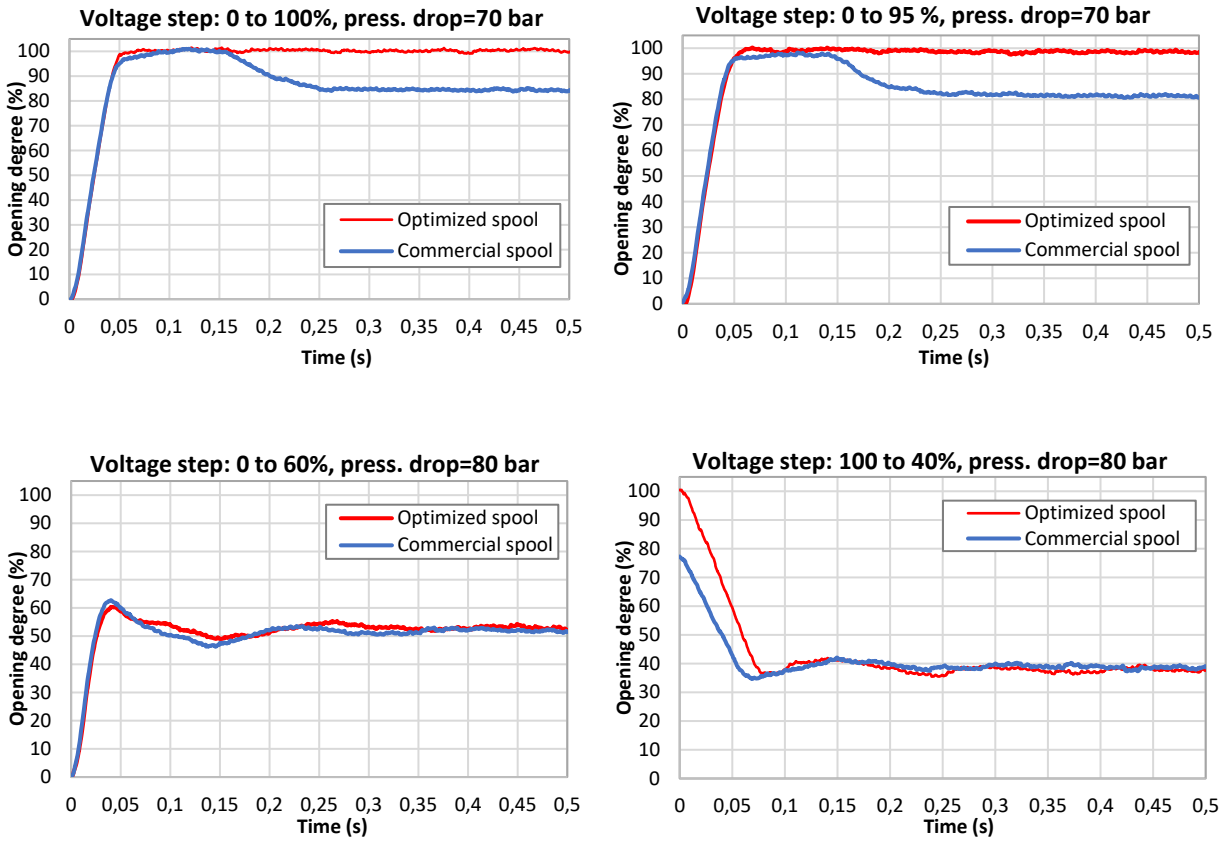

Figure 9*- Time histories of four step tests: comparison between the optimized spool (red curves) and the commercial one (blue curves)*

The graph at the top left of Figure 9 shows the time history of a first test performed with the pressure drop P-T being set to 70 bar and with the control signal being changed from zero to the maximum value accepted by the electronic driver. In this first test, the new spool and the commercial spool reached 100% and 83% of the maximum spool position, respectively. Because of the large pressure drop, the commercial spool was not capable of reaching the maximum opening degree: this must be attributed to the fact that the flow forces acting on the commercial spool are too high when the spool is approaching the large openings, as a result of the non-effective spool surface. In contrast, the new spool was capable of reaching the maximum opening degree by virtue of the improved surface, which in turn determines lower flow forces compared to the commercial configuration. The result of a greater spool position achievable with the new spool is that the flow

438 rate delivered to the actuator can be remarkably higher. In fact, the mass flow rate was measured
439 to be 1.75 kg/s for the optimized spool and 1.46 kg/sec for the commercial spool, thus increasing
440 the operation field of the valve by about 15%.
441 As far as the response time is concerned, the graph at the top left of Fig. 9 shows that the new spool
442 does not alter the transient characteristics during the rising phase, with the rise time being the same
443 in both cases. The two spools were both capable of reaching the maximum opening with the same
444 rise time because, during the opening transient, the same forces are applied in both cases: the
445 magnetic actuation force, the inertia force (the mass of the optimized spool has not significantly
446 changed compared to the commercial one) and the elastic force. While the flow forces are neglected
447 due to the very low value of flow rate, this due to the inertia of hydraulic fluid. On the contrary,
448 after the commercial spool had reached the maximum opening and consequently the flow rate had
449 reached the steady value, the high value of flow force determined by the non-optimized spool
450 surface did not allow the commercial spool to maintain this position. In fact, the commercial spool
451 moved backwards until it reached the final position given by the equilibrium between the actuation
452 force, the stationary flow force and the elastic force. Instead, the optimized spool was able to
453 maintain the maximum position and no backward motion occurred in this case, by virtue of the
454 lower flow force determined by the optimized spool surface. As a result, in addition to allowing the
455 achievement of higher opening degrees, the optimized surface also reduces the overall interval time
456 required to reach a steady position when approaching the large opening degrees.

457 The graph at the top right of Figure 9 reports the time history of a second step test consisting in
458 changing the control signal from zero to 95% of the maximum voltage accepted by the electronic
459 driver, for a pressure drop P-T equal to 70 bar. As shown by the graph, the optimized spool was
460 capable of reaching 98% of the maximum opening, whereas the commercial spool reached only 80%
461 of the maximum opening. This second step test confirms both the results of the first test and the

462 great improvement provided by the new spool in terms of opening degree and mass flow rate
463 achievable. In fact, in this second test the measured mass flow rate was equal to 1.69 kg/sec for the
464 optimized spool and 1.42 kg/s for the commercial spool: again, a large mass flow rate difference of
465 the order of 15% was registered.

466 The two step tests presented so far (and shown at the top of Fig. 9) were performed by imposing
467 high values of the control signal, revealing a great difference between the two spools. Such a large
468 difference was indeed expected, as high values of the control signal determines high opening
469 degrees, and the optimized spool surfaces were conceived to be highly effective at the large
470 openings. In contrast, as mentioned in Section 2.1, when the voltage is low and the pressure drop is
471 high, the difference between the two spools is expected to be slight, because low voltage values
472 determine small opening degrees, and the optimized spool profiles become almost ineffective at
473 the small openings. Even this behavior was confirmed by the step tests performed. In this regard,
474 the graph at the bottom left of Fig. 9 shows that, when the voltage was set to a low value (namely
475 60% of the maximum voltage), the difference between the opening degrees reached by the two
476 spools was almost negligible, with the optimized spool reaching a slightly higher axial position as
477 well as a slightly higher flow rate compared to the commercial spool. Specifically, the optimized
478 spool reached a position equal to 53.5% of the maximum opening and provided a mass flow rate of
479 0.720 kg/sec, whereas the commercial spool reached 52% of the maximum opening and provided a
480 mass flow rate of 0.705 kg/s. Even the time histories of the two spools are almost the same, with
481 both spools moving backwards after reaching about 60% of the maximum opening, because the
482 effect of the optimized surface is very little at such a small opening degree.
483 Other step tests, not reported here for space limitations, confirm the results shown above: when
484 the voltage is low, the differences between the optimized spool and commercial spool are negligible,
485 in terms of both transient characteristics and final position reached; in contrast, when the voltage

is high, the optimized spool is capable of reaching higher opening degrees (greater than 15% when the voltage is set to the maximum value and the pressure drop is very high). This behavior can be explained by the fact that the flow force reduction is generated by the increase in both $(V_{T1})_x$ and $(V_P)_x$, according to equation 3. It should be noted that the increase in the spool position determines an increase in the flow area of the metering sections but a decrease in the flow area of both the inlet section P and the outlet section T_1 (see fig. 2). As a result, at the small openings the new spool profile is not capable of increasing $(V_{T1})_x$ and $(V_P)_x$ compared to the commercial spool, because the flow areas in sections P and T_1 are too large. In contrast, at the larger openings the flow areas in sections P and T_1 remarkably decrease with the increasing opening degree, leading to a flow force reduction that increases with the spool position.

For completeness, the graph at the bottom right of Figure 9 reports two step tests consisting of a negative step (i.e. from a higher voltage value to a lower one). The pressure drop was maintained equal to 80 bar and the voltage was reduced from 100% to 40% of the maximum value. As a consequence of the voltage reduction, both spools moved backwards until they reached a very similar opening degree (about 40%). It should be noted that the optimized spool started this negative step test from the maximum opening degree, whereas the commercial spool started from an opening degree of only 80% because of the non-optimized spool surface (although at the beginning of the test the maximum voltage was applied to both spools). This test is presented in order to highlight that the optimized spool does not produce undesired effects, e.g. the incapability to reach lower axial positions starting from higher ones. It must be noted that, in this case, the sloop of the optimized spool is slightly higher than that of the commercial spool; this is due to the fact that the optimized spool starts from a higher position than the commercial spool, which results in a higher elastic force.

509 The second test typology employed the manual actuation shown in Fig. 8 and was instrumental in
510 retrieving the actuation force as a function of the spool position for both sliding spools. The pressure
511 drops were set to very high values (70 bar and 80 bar), in order to explore the difference between
512 the two spools when the flow forces are very large. It was not possible to further increase the
513 pressure drop in order not to exceed the installed power.
514 Figures 10, 11 and 12 show the comparison between the improved spool and the commercial one
515 in terms of mass flow rate and actuation force. In order to have a reliable comparison, the oil
516 temperature registered in all tests was maintained at the same level, namely 40 °C.
517 Figure 10 shows how the flow rate changes with the spool position for both spools: the curves at
518 the left of Fig.10 were retrieved maintaining a pressure drop P-T of 70 bar over the entire spool
519 stroke, while the curves at the right of Fig.10 were retrieved with a pressure drop P-T of 80 bar (the
520 blue curves refer to the commercial spool, while the red curves refer to the optimized spool). These
521 graphs reveal that the flow rate trend is the same for both spools. This behavior is consistent with
522 the employed strategy; in fact, the two spools have the same cylindrical notches and spherical
523 grooves as well as conical cutouts, and, as a result, the flow areas and hence the flow rates are
524 identical. This can also be explained by using the equation of the mass flow rate, which can be
525 written as follows [20]:

$$\dot{m}=C_{d,V}\,A_r\sqrt{2\rho\Delta p_v} \tag{5}$$

526 where A_r is the metering area, Δp_v is the pressure drop across the valve and $C_{d,V}$ is the overall
527 discharge coefficient. $C_{d,V}$ and Δp_vcan be calculated as follows [20]:
528

$$C_{d,V}=\sqrt{\frac{{C_{d,P-B}}^2\,{C_{d,A-T1}}^2}{{C_{d,P-B}}^2+{C_{d,A-T1}}^2}} \tag{6}$$

$$\Delta p_v = \Delta p_{P-A}+\Delta p_{B-T} \tag{7}$$

529 with $C_{d,P-B}$ and $C_{d,A-T1}$ being the discharge coefficients of the metering section P-B and A-T_1,
530 respectively (see Fig.2). Because both $C_{d,P-B}$ and $C_{d,A-T1}$ have not been changed (the metering
531 characteristics are the same for both spools), it results that $C_{d,V}$ (equation 6) and $\dot{m}$ (equation 5) are
532 the same for both spools.
533 The influence of the grooves, notches and cutouts upon the flow rate curves is clear when observing
534 the flow rate trends in Fig. 10: the flow rate increases with a parabolic trend due to the increasing
535 circumferential extension of the cylindrical grooves, up to a displacement equal to about 40% of the
536 maximum opening degree. When this spool position is reached, the conical cutout is uncovered and
537 the flow rate curve becomes linear and steep, since the oil can flow through the entire
538 circumference of the spool and the flow area increases linearly with the spool displacement.
539 It should be noted that the flow rate registered at 80 bar is higher than the flow rate registered at
540 70 bar for a fixed value of the spool position; in fact, using equation 5, one obtains that the ratio of
541 the flow rates ($\bar{\dot{m}}/\dot{m}$) is equal to the ratio of the pressure drops ($\overline{\Delta p_v}/\Delta p_v$)

$$\frac{\bar{\dot{m}}}{\dot{m}} = \sqrt{\frac{\overline{\Delta p_v}}{\Delta p_v}} \tag{8}$$

542 Figure 11 shows the actuation force as a function of the spool position for both spools (at the left of
543 Fig.11) and the actuation force as a function of the flow rate (at the right of Fig.11). These curves
544 refer to the test performed with the pressure drop P-T being maintained equal to 70 bar. It is
545 noteworthy that, despite the identical flow rate trends (see Fig. 10), the actuation force required to
546 move the optimized sliding spool is remarkably lower than that required to move the commercial
547 spool. The difference is null at the small openings and increases with the increasing opening degree,
548 with the maximum difference (approx. 12%) occurring at the maximum opening. These curves
549 confirm that the optimized surfaces are ineffective at the small openings and are beneficial at the
550 large openings, with the beneficial effect increasing with the increasing opening degree.

The graph at the right of Figure 11 shows that, as expected, the actuation force increases with the increasing flow rate for both spools; however, the slope of the new actuation force is remarkably lower than the commercial one. As a result, the maximum actuation force required in the new spool configuration (12.5 daN) is capable of producing a mass flow rate of 1.75 kg/s and an opening degree of 100%, whereas the same force level can produce a mass flow rate of only approx. 1.46 kg/s and an opening degree of 84% in the commercial configuration. These results are noteworthy, as the flow rate difference is of the order of 15%, and confirm the results provided by the first step test (see the graph at the top left of Fig. 9).

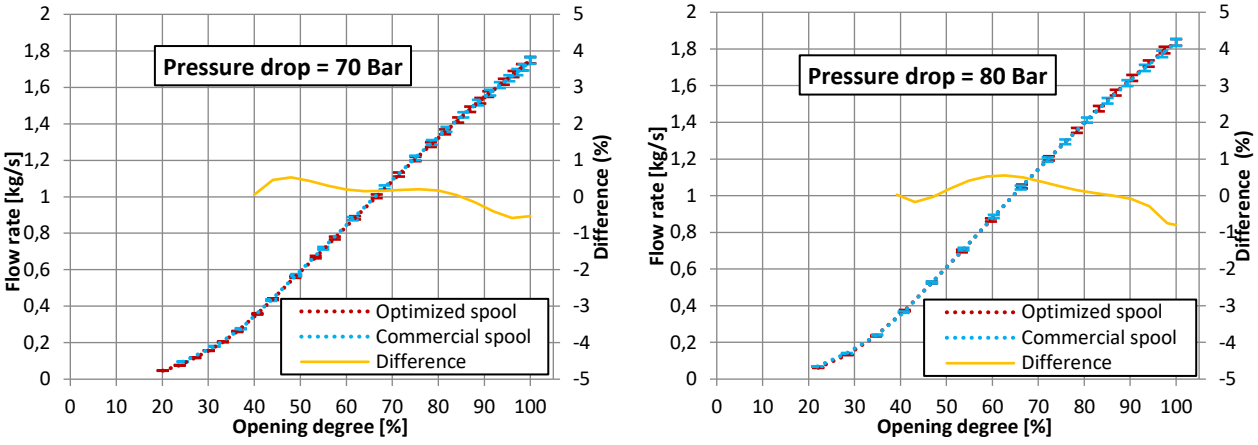

Figure 10 *– Flow rate vs spool position (left: pressure drop=70 bar; right: pressure drop=80 bar): comparison between the optimized spool (red curve) and the commercial spool (blue curve)*

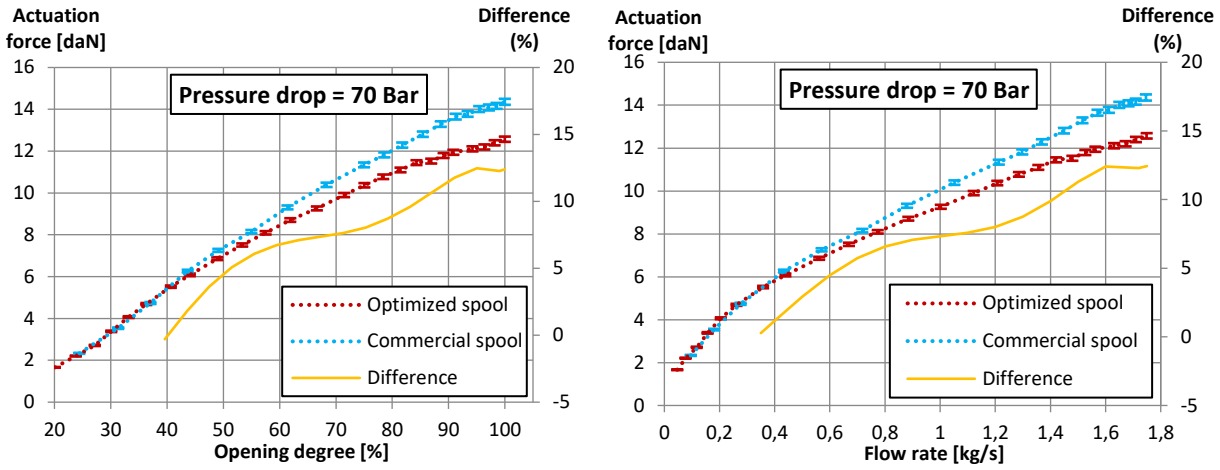

564

565 ***Figure 11***– *Actuation force vs spool position (left) and actuation force vs flow rate (right) for a*

566 *pressure drop of 70 bar: comparison between the optimized spool (red curve) and the commercial*

567 *spool (blue curve)*

568 Figure 12 shows the comparison between the actuation forces required by the optimized spool (red

569 curves) and the commercial one (blue curves) for a fixed pressure drop equal to 80 bar. The

570 comparison performed at 80 bar gave the same results as those achieved at 70 bar; in fact, the

571 actuation force curves retrieved at 80 bar confirm the large actuation force reduction achieved with

572 the new spool. Figure 12 shows that the maximum actuation force registered with the optimized

573 spool is equal to 13.2 *daN*; this force level can determine an opening degree of only approx. 83%

574 when the commercial spool is used, confirming the results presented so far. Figure 12 also confirms

575 that the new spool profile, compared to the commercial one, remarkably lowers the slope of the

576 actuation force as a function of the volumetric flow rate. In this case, the maximum actuation force

577 measured with the new spool configuration (13.2 *daN*) is capable of achieving a mass flow rate of

578 about 1.84 *kg/s*, whereas the same force level can produce a mass flow rate of only about 1.55 *kg/s*

579 in the commercial configuration. Again, the improvement is noteworthy, as the flow rate difference

580 is greater than 15%.

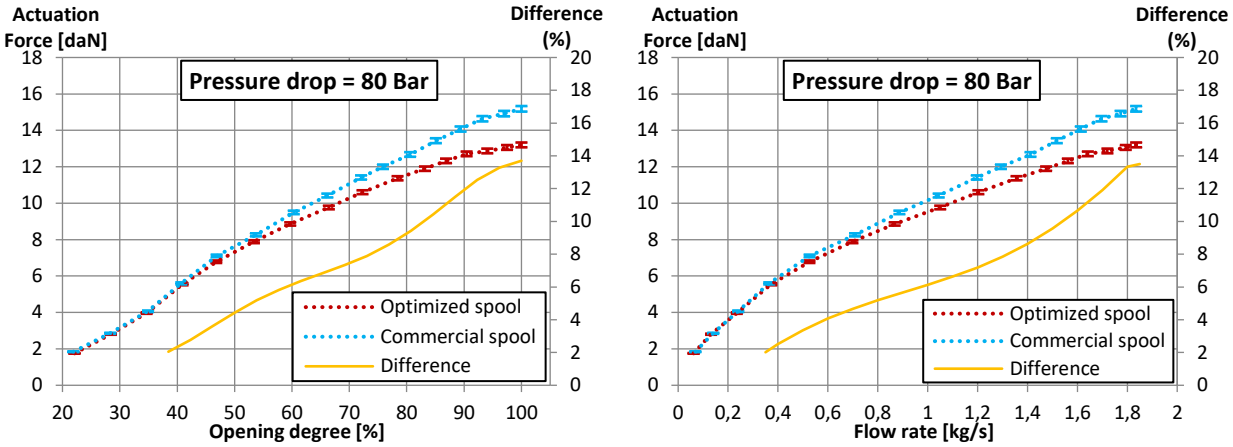

581

582 ***Figure 12***– *Actuation force vs spool position (left) and actuation force vs flow rate (right) for a*

583 *pressure drop of 80 bar: comparison between the optimized spool (red curve) and the commercial*

584 *spool (blue curve)*

585 Table 2 reports the comparison between the experimental actuation forces and the numerical ones,

586 with the latter having been achieved by summing the elastic forces of the centering springs and the

587 flow forces predicted by the CFD model described in [24] and implemented into the optimization

588 process [27]. The numerical model seems to slightly under-estimate the flow force reduction in

589 comparison with the experimental data; this under-estimation results from the difference existing

590 between the numerical data and the experimental predictions, which is of the order of 4÷5%, as

591 also shown in [20].

592 The values chosen and reported in Table 2 regard the opening degree corresponding to a spool

593 travel of 2.55 *mm*, which is the same opening degree employed in the optimization process [26]. To

594 allow the comparison between the experimental results and the numerical ones, in the simulations

595 the pressure drop P-T was set to 70 bar, while the pressure drop B-A (due to the gear flow meter –

596 n. 2 in figure 7) was reproduced by means of the pressure jump condition [24].

597

	Commercial spool *(N)*	Optimized spool *(N)*	Percentage improvement
Experimental actuation force	137.0	121.1	11.6%
Numerical actuation force (single phase model)	132.5	123.0	7.2%

598

599 Table 2- Comparison between the numerical actuation forces and the experimental ones (opening
600 degree = *2.55 mm*)

601 **4. Conclusion**

602 This paper has presented the experimental comparison between a commercial sliding spool and an
603 improved one, which was designed using new spool profiles that allow the flow force and hence the
604 actuation force to be reduced. The difference between the new spool and the commercial one is
605 that the new compensation profile and the new lateral conical surfaces of the spool allow increasing
606 the axial velocity at the inlet of the metering chamber P-B and at the outlet of the metering chamber
607 A-T, which in turn allow decreasing the flow force according to the momentum equation. The new
608 spool was designed by maintaining the same metering characteristics, in order not to change the
609 flow rate trend vs the spool position. The new design concept has general validity and can be applied
610 to any four way three position direct operated proportional directional valve, considering that very
611 similar architectures for these valves are used by manufacturers.
612 In order to perform the experimental comparison between the commercial spool design and the
613 proposed one, the commercial valve body was inserted in a hydraulic circuit, which was made up of
614 a pump, an accumulator, a proportional pressure relief valve, four pressure transducers and a flow
615 meter. Two typologies of experimental tests were carried out: the first one consisted in moving the
616 spool by means of the electronic driver provided by the manufacturer, whereas the second test
617 typology consisted in using a manual actuation system that allowed the actuation force to be
618 accurately measured by a load cell.

The first test typology was instrumental in recognizing which spool reached the largest opening degree for a fixed value of the control signal and pressure drop. The step tests showed that the new spool is capable of reaching remarkably higher axial positions, evidencing that the potential of the valve is enhanced by the new spool profile.

The second test typology was instrumental in retrieving the flow rate vs the spool position, the actuation force vs the spool position and the actuation force vs the flow rate for both spools. These curves were retrieved for fixed and very high pressure drops (namely 70 and 80 bar). The comparison between the experimental curves of the new spool and those of the commercial one reveals that the flow rate is identical in both cases, whereas the actuation force required to move the new spool is remarkably lower than that required by the commercial one, with the actuation force difference being greater than 10% at the maximum opening. Moreover, for a fixed actuation force level, the maximum difference in terms of flow rate is greater than 15%.

Acknowledgements

The authors thanks Cesare De Palma and Nico De Palma with Danilo De Palma (Managers of De.Ol. and Icosystems companies, respectively), as well as Michele Mizzi and Vito Mele for their support in the experimental campaign.

References

1. Sangiah, D. K., Plummer, A. R., Bowen, C. R., & Guerrier, P. (2013). A novel piezohydraulic aerospace servovalve. Part 1: design and modelling. Proceedings of the Institution of Mechanical Engineers, Part I: Journal of Systems and Control Engineering, 227(4), 371-389.
2. Bertin, M. J. F., Plummer, A. R., Bowen, C. R., & Johnston, D. N. (2014, September). An Investigation of Piezoelectric Ring Benders and Their Potential for Actuating Servo Valves. In

643 ASME/BATH 2014 Symposium on Fluid Power and Motion Control (pp. V001T01A034-
644 V001T01A034). American Society of Mechanical Engineers.
645 3. Chattopadhyay, H., Kundu, A., Saha, B. K., & Gangopadhyay, T. (2012). Analysis of flow
646 structure inside a spool type pressure regulating valve. Energy Conversion and Management,
647 53(1), 196-204.
648 4. Saha, B. K., Chattopadhyay, H., Mandal, P. B., & Gangopadhyay, T. (2014). Dynamic
649 simulation of a pressure regulating and shut-off valve. Computers & Fluids, 101, 233-240.
650 5. Loha C., Chattopadhyay H., Chatterjee P.K. Euler-Euler CFD modeling of fluidized bed:
651 Influence of specularity coefficient on hydrodynamic behavior, Particuology, 11 (6), 2013,
652 pp. 673-680.
653 6. Qian JY, Zhang H, Wang JK. Research on the optimal design of a pilot valve controlling cut-
654 off valve. Applied Mechanics and Materials 2013; 331: 65–9.
655 7. Qian JY, Wei L, Jin ZJ, Wang JK, Zhang H, Lu A. CFD analysis on the dynamic flow
656 characteristics of the pilot-control globe valve. Energy Conversion and Management 2014;
657 87: 220–226
658 8. Aung, N. Z., Yang, Q., Chen, M., & Li, S. (2014). CFD analysis of flow forces and energy loss
659 characteristics in a flapper–nozzle pilot valve with different null clearances. Energy
660 Conversion and Management, 83, 284-295.
661 9. Pan, X., Wang, G., & Lu, Z. (2011). Flow field simulation and a flow model of servo-valve spool
662 valve orifice. Energy Conversion and Management, 52(10), 3249-3256.
663 10. Aung, N. Z., & Li, S. (2014). A numerical study of cavitation phenomenon in a flapper-nozzle
664 pilot stage of an electrohydraulic servo-valve with an innovative flapper shape. Energy
665 Conversion and Management, 77, 31-39.

11. Yang, Q., Aung, N. Z., & Li, S. (2015). Confirmation on the effectiveness of rectangle-shaped flapper in reducing cavitation in flapper–nozzle pilot valve. Energy Conversion and Management, 98, 184-198.
12. Zhang, S., & Li, S. (2015). Cavity shedding dynamics in a flapper–nozzle pilot stage of an electro-hydraulic servo-valve: Experiments and numerical study. Energy Conversion and Management, 100, 370-379.
13. Zhang, S., Aung, N. Z., & Li, S. (2015). Reduction of undesired lateral forces acting on the flapper of a flapper–nozzle pilot valve by using an innovative flapper shape. Energy Conversion and Management, 106, 835-848.
14. Lisowski, E., & Rajda, J. (2013). CFD analysis of pressure loss during flow by hydraulic directional control valve constructed from logic valves. Energy Conversion and Management, 65, 285-291.
15. Herakovič, N. (2009). Flow-force analysis in a hydraulic sliding-spool valve. Strojarstvo: časopis za teoriju i praksu u strojarstvu, 51(6), 555-564.
16. Simic, M., & Herakovic, N. (2015). Reduction of the flow forces in a small hydraulic seat valve as alternative approach to improve the valve characteristics. Energy Conversion and Management, 89, 708-718.
17. Herakovič, N., Duhovnik, J., & Šimic, M. (2015). CFD simulation of flow force reduction in hydraulic valves. Tehnicki vjesnik/Technical Gazette, 22(2), 555-564.
18. Lisowski, E., Czyżycki, W., & Rajda, J. (2013). Three dimensional CFD analysis and experimental test of flow force acting on the spool of solenoid operated directional control valve. Energy Conversion and Management, 70, 220-229.

688 19. Šimic, M., Debevec, M., & Herakovič, N. (2014). Modelling of hydraulic spool-valves with
689 special designed metering edges. Strojniški vestnik-Journal of Mechanical Engineering, 60(2),
690 77-83.
691 20. Amirante, R., Distaso, E., & Tamburrano, P. (2014). Experimental and numerical analysis of
692 cavitation in hydraulic proportional directional valves. Energy Conversion and Management,
693 87, 208-219.
694 21. Amirante, R., Innone, A., & Catalano, L. A. (2008). Boosted PWM open loop control of
695 hydraulic proportional valves. Energy Conversion and Management, 49(8), 2225-2236.
696 22. Jin, B., Zhu, Y. G., Li, W., Zhang, D. S., Zhang, L. L., & Chen, F. F. (2014). A differential control
697 method for the proportional directional valve. Journal of Zhejiang University SCIENCE C,
698 15(10), 892-902.
699 23. Ye, Y., Yin, C. B., Li, X. D., Zhou, W. J., & Yuan, F. F. (2014). Effects of groove shape of notch
700 on the flow characteristics of spool valve. Energy Conversion and Management, 86, 1091-
701 1101.
702 24. Amirante, R., Catalano, L. A., & Tamburrano, P. (2014). The importance of a full 3D fluid
703 dynamic analysis to evaluate the flow forces in a hydraulic directional proportional valve.
704 Engineering Computations, 31(5), 898-922.
705 25. Atos spa, 21018 Sesto Calende, Italy; https:// www.atos.com (accessed in September 2015).
706 26. Amirante, R., Catalano, L. A., Poloni, C., & Tamburrano, P. (2014). Fluid-dynamic design
707 optimization of hydraulic proportional directional valves. Engineering Optimization, 46(10),
708 1295-1314.
709 27. Amirante, R., & Tamburrano, P. (2015). Novel, cost-effective configurations of combined
710 power plants for small-scale cogeneration from biomass: Feasibility study and performance
711 optimization. Energy Conversion and Management, 97, 111-120.